
Contents

1	Introduction to structural impact	1
1.1	Features of impact phenomena	6
1.1.1	Inertia effects	6
1.1.2	Material response	7
1.1.3	Transient effects	9
1.1.4	Stability	10
1.1.5	Failure	11
1.2	Crashworthiness	12
1.3	Experimental techniques	14
1.4	Analytical and computational methods	18
1.4.1	Analytical versus numerical solutions	19
1.5	A bit of history	21
1.6	Engineering ethics	22
1.7	Book organization	24
1.8	Problems	25
2	Rigid body impact	27
2.1	Impulse and momentum of a single particle	30
2.2	Coefficient of restitution	34
2.3	Oblique central impact	39
2.4	In plane rigid body dynamics: eccentric impact	43

2.5	Filming impact events	50
2.5.1	Motion analysis	52
2.6	Closure	52
2.7	Problems	53
3	One-dimensional elastic waves and impact of bars	57
3.1	Strain-stress waves	58
3.2	Axial collinear impact of two equal semi-infinite bars	66
3.3	Reflection of waves	68
3.4	Impact of two finite bars	70
3.5	Free vibration of bars	75
3.6	Forced vibration of bars	81
3.7	Visco-elastic waves: dispersion	85
3.7.1	Geometrical dispersion	87
3.8	Measurement of motion	89
3.8.1	Foil strain gauges	90
3.8.2	Accelerometer and load cells	93
3.8.3	Laser Doppler vibrometer	94
3.9	Closure	96
3.10	Problems	96
4	Elasto-dynamics of beams	99
4.1	Equilibrium equation for beams	100
4.2	Free vibration	103
4.3	Dynamics of elastic beams to initial conditions	106
4.4	Impact of a mass on a beam	113
4.5	Dynamic response of beams to a force	117
4.6	Flexural waves	119
4.6.1	Rayleigh and Timoshenko beam theories	121
4.7	Digital signals	123
4.7.1	Fourier series and Fourier transform	127
4.7.2	Discrete Fourier transform	133
4.7.3	Filters	136
4.8	Closure	138
4.9	Problems	138

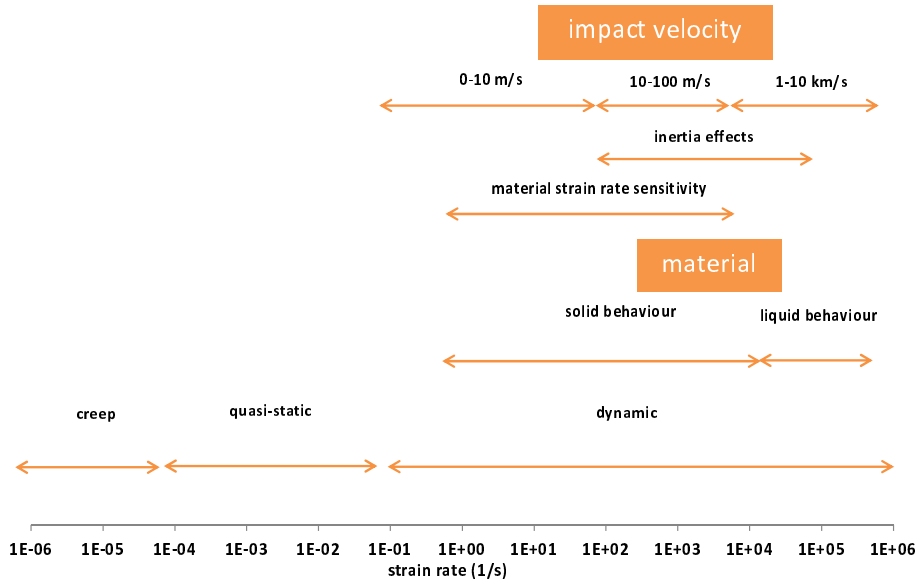
5	Visco-plastic dynamics of beams and plates	141
5.1	Plastic behaviour of beams	142
5.1.1	Perfectly plastic material model	142
5.1.2	Beam collapse load	144
5.1.3	Yield surface	148
5.2	Central impact in a beam	152
5.3	Beam loaded by a pressure pulse	157
5.4	Equivalent pulse	163
5.5	Transverse shear effects	166
5.6	Large displacements effects	171
5.7	Strains and strain rate in beams	175
5.7.1	Strains	176
5.7.2	Strain rate	179
5.8	Circular plates impulsively loaded	180
5.8.1	Equilibrium equations	181
5.8.2	Critical velocity	184
5.8.3	Motion after severance — moving hinge phase	185
5.8.4	Motion after severance — hinge at the center	188
5.8.5	Rigid body motion	190
5.9	Circular plates under low velocity impact of a mass	193
5.10	Plates under high velocity impact of a mass: ballistic limit	196
5.11	Experiments on beams and plates	198
5.12	Closure	202
5.13	Problems	202
6	Axial impact in shells and plastic waves	205
6.1	Dynamic buckling of a bar	206
6.2	Dynamic buckling of cylindrical shells	209
6.3	Plastic waves in bars	210
6.4	Plastic waves in cylindrical shells	218
6.4.1	Peak load in a tube	222
6.5	Progressive buckling of cylindrical shells	224
6.6	Progressive buckling of rectangular tubes	229
6.7	Experiments with shells: buckling transition	236
6.8	Closure	241
6.9	Problems	241

7	Material behaviour and failure	243
7.1	Stress–strain definitions	245
7.2	Tensile tests	250
7.2.1	Equivalent (effective) stress and strain	252
7.2.2	Necking	254
7.3	Compression tests	256
7.4	Medium strain rate tests	257
7.5	High strain rate tests	258
7.5.1	Dispersion	263
7.5.2	Friction correction	264
7.5.3	Inertia and punching effects correction	266
7.6	Material constitutive laws	267
7.7	Inverse modelling and image analysis	274
7.8	Yield criterion	276
7.8.1	Normality and consistency condition	283
7.8.2	Isotropic strain hardening	285
7.9	Material failure	286
7.10	Closure	292
7.11	Problems	293
8	Linear Finite Elements Analysis	295
8.1	The finite element method in dynamics: explicit and implicit	296
8.2	Finite elements for beams	303
8.2.1	Quasi–static loads	303
8.2.2	Dynamic loading: forced response	312
8.2.3	Modal analysis	315
8.3	An axisymmetric finite element	316
8.3.1	Basic formulas	317
8.3.2	Rectangular finite element	320
8.3.3	Isoparametric formulation	322
8.3.4	Numerical integration	325
8.3.5	Stress calculation	328
8.4	Closure	329
8.5	Problems	329
9	Nonlinear Finite Elements Analysis	331
9.1	Nonlinear truss element	332
9.2	Newton–Raphson procedure	337
9.3	A non–linear beam finite element	341

9.3.1	Tangent matrix	346
9.4	One dimensional computational plasticity	347
9.4.1	Unidimensional return mapping (radial) algorithm	351
9.5	Kinematics of large deformations	354
9.5.1	Rate of deformation	358
9.6	Stresses	359
9.7	Stress rates	360
9.8	Plastic deformation gradient	363
9.9	Computational plasticity – three dimensional case	364
9.10	Closure	367
9.11	Problems	367
10	Scaling	369
10.1	Size in nature	370
10.2	Relating model to prototype	372
10.3	Analytical example	378
10.4	Numerical example	380
10.5	Model and prototype made of different materials	381
10.6	Geometrically distorted scaled models	388
10.7	Scaling of distorted models using finite elements	393
10.8	Closure	395
10.9	Problems	395
11	Impact engineering	397
11.1	Tyre impact	398
11.1.1	Experimental and numerical set-up	399
11.1.2	Results	401
11.2	Optimizing a compressor to resist a fall	402
11.3	High velocity impact in metal plates	404
11.3.1	Material properties and ballistic tests	405
11.3.2	Finite element model	407
11.4	Ship collision	409
11.4.1	T cross-section beams	413
11.4.2	Frontal ship collision against rigid wall	415
11.4.3	Lateral ship-to-ship collision	416
11.5	Collision of a car against a guardrail	417
11.5.1	Collision against a concrete barrier	423
11.6	Final conclusions	424
11.7	Problems	425

tation.

We can conceive a classification of the various impact events, as in the next figure.



A general classification of structural impact based on the strain rate, which is proportional to the impact velocity.

The most obvious approach would be to use the impact velocity as the major variable dictating the type of impact and its consequences. The objects involved in the impact may also serve for classification purposes. It can be seen that impact can take place, for instance, among objects that do not deform much, such as the classic impact between two billiard balls. This rigid impact event is in contrast with the impact of a ball hitting a flexible beam, leading the latter to vibrate. In this elastic impact event, the propagation of waves along the structure is an important feature that needs to be taken into account. Another common type of impact is when the colliding bodies deform permanently, like the impact of two cars. This impact event is usually associated with large permanent deformation of the material.

In the cases above, the impact velocity is crucial in determining the structure behaviour and we refer to high and hyper velocity impact, the former being, for instance, the impact of a bullet (say 600 m/s) and the latter the impact of a meteorite on a space station (say 20 km/s).

In a general classification some phenomena are manifested in a more pronounced way. For instance, in impact events at low velocity, we shall

Scientists at Sandia National Laboratories, in USA, blasted in 1994 a small projectile to a speed of 18 km/s. This is one of the highest velocities ever reached by an object on earth.

Basically, in the former method, one strives to solve the equilibrium equation of a structure in its differential form while in the FEM the equations are of algebraic nature. This requires simple procedures, *eg* Gauss elimination, to solve a system of equations whose unknowns are the displacements of various points (domain) of a structure. Such a procedure can be carried out along time so one has a complete description of the structure motion in space and time.

The immediate question that arises is why to develop further analytical models. Why not to use exclusively FEM structural analysis?

The answers to these questions are manifold. First of all, analytical solutions can disclose features of a phenomenon that are presented in the numerical solution but that are not evident to the analyst. A good example in the context of this book is the axial impact of a mass on a tube. We shall see in Chapter 6 that it is possible to obtain a simple expression for the peak load, for a given material, geometrical and impact conditions, which are useful in the design of a shock absorber. If one opts for the FEM it is necessary to run various cases until a given design bound is met.

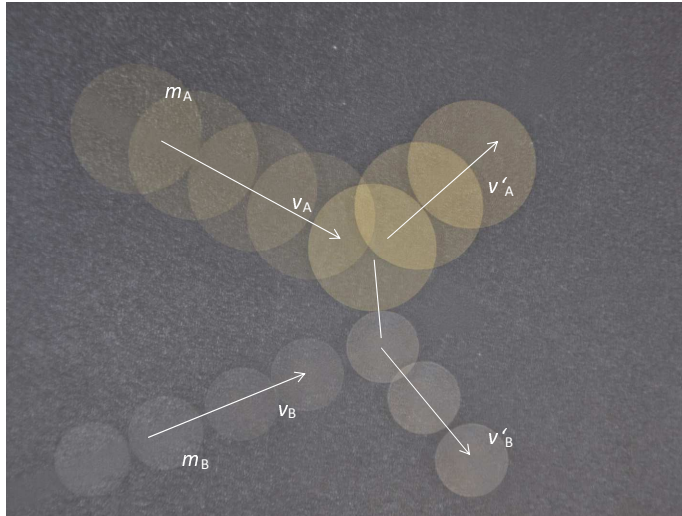
There are many other examples along these lines which will be discussed in this book. For now we bring another point of view into the discussion.

The FEM is capable of yielding accurate solutions but at least three aspects should be known in advance: the way the structure is supported, the intensity in time of the loads and the response of the material from which the structure is made. All these aspects are difficult to be known precisely, in striking contrast with the precision of the analyses tool used, *ie* here FEM. Hence, in many cases, given the lack of knowledge on the above variables, a more straightforward analytical solution can give acceptable results.

There is perhaps a more subtle argument for the study of analytical models. Analytical solutions require a dose of imagination. FEM modelling requires operational procedures, greatly simplified by powerful graphical interfaces between the analyst and the computer. Also, if one does not learn the fundamentals of the FEM, via an analytical approach, no further progress is possible in the numerical area.

Many important problems can be solved by elementary equations steamed from basic mechanics laws. To model a problem and to choose the right equations to describe it, hinges on the imaginative process of

See M.L. Bucleam and K. Bathe, *The Mechanics of Solids and Structures — Hierarchical Modelling and the Finite Element Solution*, Springer, 2011 and N. Jones, *The credibility of predictions for structural designs subjected to large dynamic loadings causing inelastic behaviour*, *International Journal of Impact Engineering*, 53, pp. 106–114, 2013.



Oblique impact of two disks moving on a frictionless surface.



IMPACT OF TWO DISKS

Consider the impact of two flat disks moving on a frictionless surface as in the next figure and evaluate their final velocities. Assume a coefficient of restitution e .

Since $v'_{B_n} - v'_{A_n} = e(v_{A_n} - v_{B_n})$, we write for the normal direction, n ,

$$m_A v_{A_n} + m_B v_{B_n} = m_A v'_{A_n} + m_B [v'_{A_n} + e(v_{A_n} - v_{B_n})],$$

from which it follows, with $m_r = m_A/m_B$, that,

$$v'_{A_n} = \frac{1}{1 + m_r} [(m_r - e)v_{A_n} + (1 + e)v_{B_n}]$$

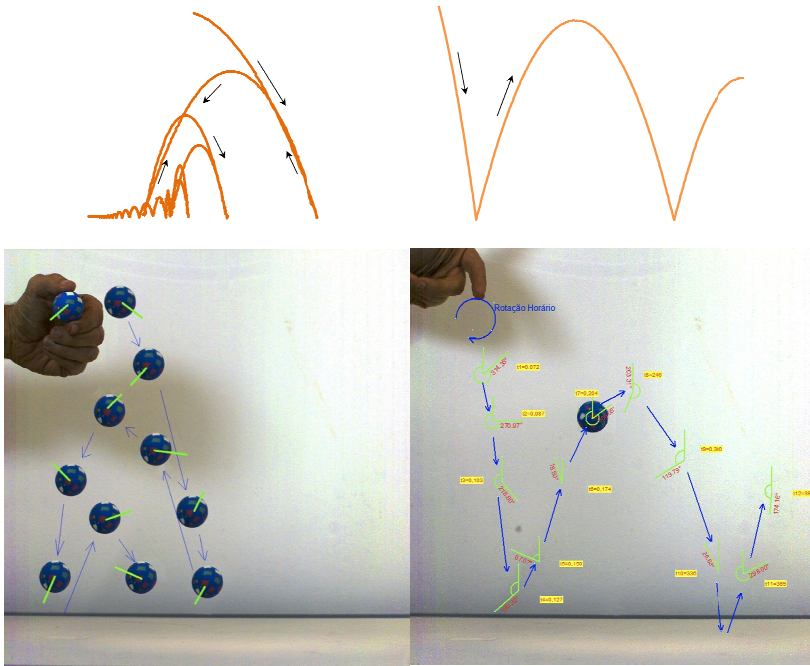
and

$$v'_{B_n} = (1 + e)m_r v_{A_n} + (1 - em_r)v_{B_n},$$

with $v_{A_n} = v_A \sin \alpha$ and $v_{B_n} = v_B \sin \alpha$, being α the angle between v_A and v_B . Of course that $v_{A_t} = v'_{A_t}$ and $v_{B_t} = v'_{B_t}$



There are some practical problems where the colliding objects have their motion somehow restrained, as illustrated in the next figure. Again



A rotating ball launched counter clockwise (left) and clockwise (right).

of the rod plus of the bullet just after impact, see next figure, from which it follows that

$$m_b v_b l \cos \alpha = m_b l v'_{b_x} + m_r \bar{v}'_r L/2 + \bar{I} \omega'$$

The use of the coefficient of restitution yields

$$v'_r - v'_{b_x} = e v_b \cos \alpha,$$

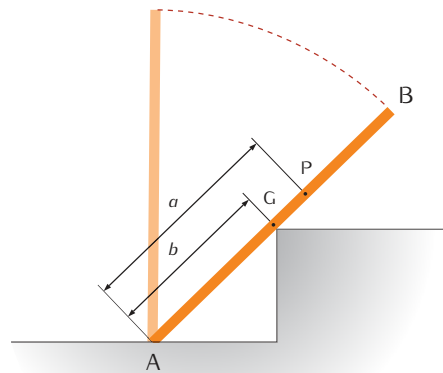
which, together with the previous equation gives

$$\omega' = \frac{3l m_b v_b \cos \alpha (1 + e)}{3m_b l^2 + m_R L^2} \quad \text{and} \quad v'_{b_x} = v_b \cos \alpha \left(\frac{3m_b l^2 - m_R L^2 e}{3m_b l^2 + m_R L^2} \right).$$

The final velocity is the vector addition of v'_{b_x} and $v'_{b_y} = v_b \sin \alpha$.

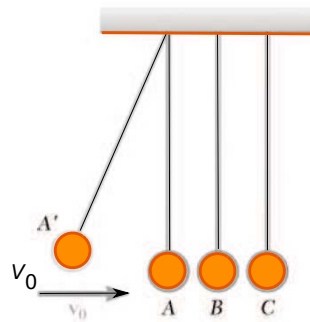
The reactive impulse in the x direction comes from $m_b v_b \cos \alpha + F_x \Delta t = m_S v'_{b_x} + m_R \bar{v}'_R$, giving

$$\bar{I}_x = F_x \Delta t = (1 + e) m_b m_R v_b \cos \alpha L \left(\frac{3l/2 - L}{3m_b l^2 + m_R L^2} \right),$$



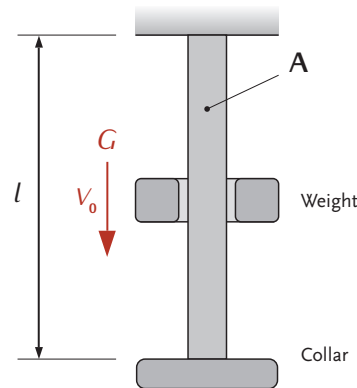
A rod hitting a corner.

8. Considering a row of n spheres held by strings, as in the figure below, obtain the velocity of the last sphere assuming an initial impact velocity V_0 and a coefficient of restitution e between any pair of spheres.



A row of spheres being hit by the first one.

9. A block moving on a frictionless surface with velocity v collides against stationary identical block with an angle α between the common normal direction and the path of the travelling block. Evaluate the deflected angle of the two blocks as a function of the restitution coefficient e .
10. Based on the next figure, determine the final velocity of block A and sphere B as a function of the angles shown.



A mass hitting a bar.

The strain energy in the wire when equated to the kinetic energy gives

$$Al \int \varepsilon d\sigma = \frac{Al\sigma^2}{2E} = \frac{GV_0^2}{2} \rightarrow \sigma = \sqrt{\frac{GE\rho}{m}} V_0.$$

The stress level according to the wave theory is

$$\sigma_d = \sqrt{E\rho} V_0,$$

so that

$$\frac{\sigma_d}{\sigma} = \sqrt{\frac{m}{G}}.$$

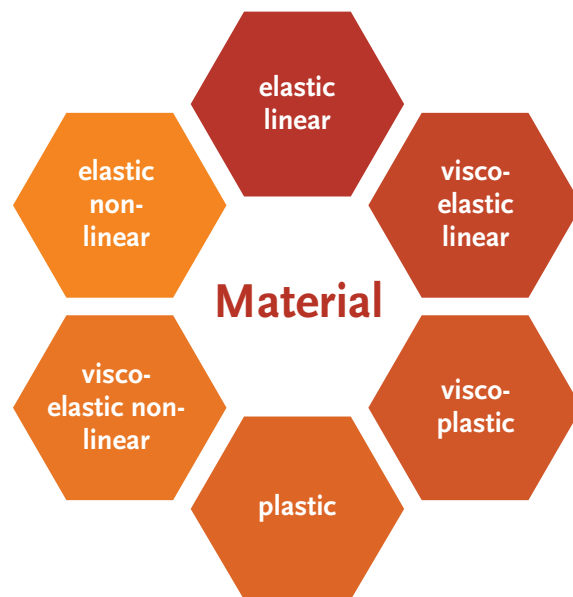
For a small striking mass, G , the actual stress can be many times larger than the one obtained by the strength of materials approach. Note that the stress level depends largely on the impact velocity.



The problem above is not completely solved because wave reflection at the extremes of the bar has not been taken into account. We will come back to this problem in the sequence and will be able to understand what the Hopkinsons, father and son, at the turn of the nineteenth–twentieth century, concluded: that the wire breaks at the suspension point and not at the impact point. They found that the wire rupture does not depend on the falling mass but rather on its velocity.

3.7 Visco-elastic waves: dispersion

Hookean materials, *ie* the ones which obey, in the uniaxial case, the constitutive law $\sigma = E\varepsilon$, are not able to represent many materials we daily use in devices and structures well. Take for instance a polymeric string. If a mass is hanged by it, it may displace further and further as time passes by and this is indicative of the so called visco-elastic material response, not contemplated by the Hook law for the lack of the parameter time. Indeed, there are a myriad of materials; science and technology strive to develop constitutive laws so structures made with them can be correctly analysed. The next figure gives an account of some common material models.



Some material models.

To model the behaviour of materials that are time dependent, a common practice is to use a set of springs and dashpots, assembled in a way thought to represent some measured response. For instance, the use of one spring and one dashpot working in parallel, known as Kelvin-Voigt model, can represent the phenomenon of creep, defined as the solid deformation under the action of a, usually constant, stress whose magnitude is lower than the flow stress.

with

$$F(\omega) = \int_{-\infty}^{\infty} f(t)e^{-i\omega t} dt$$

being the Fourier transform of our function, $f(t)$.

This equation has the important characteristic of representing a function in the frequency domain rather than in time, allowing us to obtain the spectrum of a signal, *ie* its representation in terms of frequency. Of course we measure a signal in time, but with the Fourier transformation we readily represent it in the frequency domain. This is useful in many ways since the frequency content of a signal can disclose interesting aspects that are not evident in the time domain.

Observe that the Fourier transform is a complex number. Accordingly, we write

$$F(\omega) = \int_{-\infty}^{\infty} f(t)e^{-i\omega t} dt = \int_{-\infty}^{\infty} f(t) \cos \omega t dt + i \int_{-\infty}^{\infty} -f(t) \sin \omega t dt,$$

or

$$F(\omega) = A(\omega) + iB(\omega),$$

with

$$\underbrace{|F(\omega)| = \sqrt{A(\omega)^2 + B(\omega)^2}}_{\text{modulus}} \quad \underbrace{\phi(\omega) = \tan^{-1} \frac{B(\omega)}{A(\omega)}}_{\text{phase}}$$

which are the modulus and the phase of the transformed signal at the given frequency.

Note that in the case of Fourier series of a periodic signal, we obtain the amplitude of the various harmonic that are associated with discrete values of frequency. In the case of the Fourier transform of a non-periodic signal, the spectrum is defined for all real values of frequency.



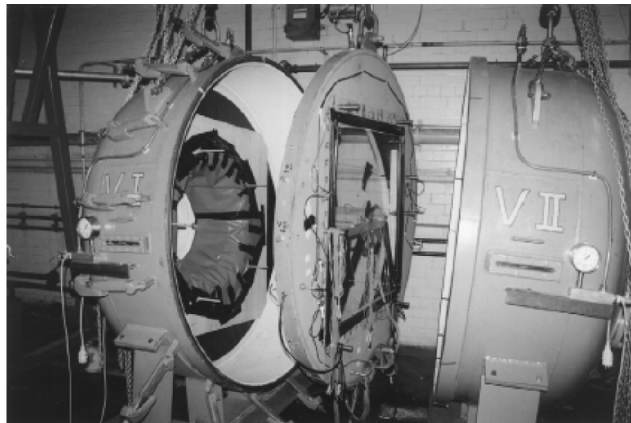
FOURIER TRANSFORM AND SERIES

Obtain the Fourier transform and the Fourier series coefficients for the function depicted in the next figure.

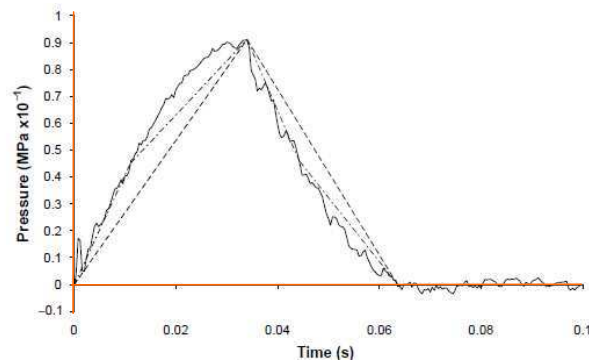
The Fourier transform (of the non-periodic function) is calculated from

$$\begin{aligned} F(\omega) &= \int_{-1}^0 (t+1)e^{-i\omega t} dt + \int_0^1 (-t+1)e^{-i\omega t} dt = \\ &= \frac{2}{\omega^2}(1 - \cos \omega) = \frac{2}{\omega^2} 2 \sin^2 \frac{\omega}{2}, \end{aligned}$$

two volumes which are then subjected to equal values of air pressure. This does not displace the panel to any side. At the opposite end of the pannel, one of the chambers has a kind of inspection window covered with a a soft sheet of a paper like material. An electrical resistance can easily tear this paper and pressurized air is suddenly released to the environment. Since the other chamber is still pressurized this generates a load difference in the panel, which responds eventually with permanent deformation.

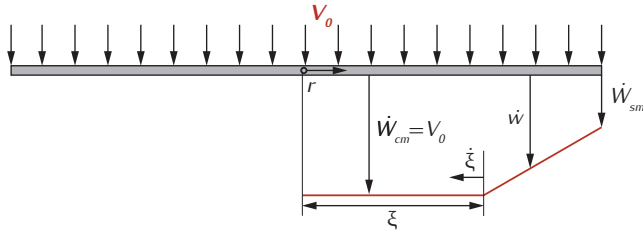


(a) A rig to apply a pressure pulse in plates and (b) an actual pressure pulse. From G.K. Schleyer, S.S. Hsu, M.D. White and R.S. Birch, Pulse pressure loading of clamped mild steel plates, *International Journal of Impact Engineering*, 28, p. 223–247, 2003.



As evident from the figure, this pressure pulse does not resemble the rectangular one used in the analyses of the previous sections. Had we used it, the integrations of the equations of motion would be further complicated. Hence, it would be very useful to transform a real pulse into an equivalent rectangular one. To this end, consider the definition

Post-severance velocity profile in the moving hinge phase for a circular plate with $\nu \geq 2$.



which can be integrated once and, using $M_\theta = M_0$, gives

$$Q_r = \frac{1}{r} \left(\mu \int r \ddot{w} dr - M_0 + c_1 \right),$$

or

$$Q_r = \frac{\mu \ddot{W}_{sm}}{R - \xi} \left(\frac{r^2}{3} - \frac{\xi r}{2} + \frac{\xi^3}{6r} \right) + \frac{\mu(V_0 - \dot{W}_{sm})\dot{\xi}}{(R - \xi)^2} \left(\frac{Rr}{2} - \frac{r^2}{3} - \frac{\xi^2 R}{2r} + \frac{\xi^3}{3r} \right),$$

since $Q_r|_{r=\xi} = 0$.

The transverse shear force, Q_r , is zero at the support and noting that $\frac{R^2/6 - \xi^2/2 + \xi^3/3R}{R^2/3 - \xi R/2 + \xi^3/6R} = \frac{R+2\xi}{2R+\xi}$, we obtain

$$\ddot{W}_{sm} = -\frac{(V_0 - \dot{W}_{sm})\dot{\xi}}{(R - \xi)} \frac{(R + 2\xi)}{(2R + \xi)},$$

which can be written as $\ddot{W}_{sm} = (d\dot{W}_{sm}/d\xi)\dot{\xi}$ and integrated to yield

$$V_0 - \dot{W}_{sm} = \frac{\beta \Xi}{(2R + \xi)(R - \xi)}$$

since $\dot{W}_{sm} = \dot{W}_s$ when the hinge is at $\xi = \xi_0$ and defining

$$\Xi = (2R + \xi_0)(R - \xi_0).$$

Now,

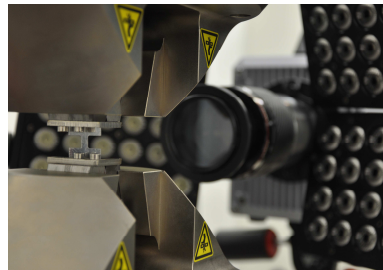
$$M_r = M_0 + \frac{1}{r} \int r Q_r dr + \frac{c_2}{r},$$

or

$$M_r = M_0 - \frac{\mu \dot{\xi} \beta}{(R - \xi)^3} \frac{\Xi}{(2R + \xi)} \times$$

CHAPTER 7

Material behaviour and failure



A camera–light system
filming a material test.

We have seen in Chapter 3 that the material behaviour bridges the kinematic and equilibrium equations of a structure. These differential equilibrium equations and their associate kinematic fields have long been established in the 19th. and 20th. centuries for many basic structures. But, as new materials are being conceived daily, it is always necessary to develop accurate mathematical models to describe their behaviour. With this in mind, the so called constitutive equations need constant improvement to reflect some odd material behaviour, as the ones depicted in the next figure.

Perhaps here is the best Chapter to bear in mind the importance of the material behaviour as the one bridging equilibrium and kinematics.

A ring (washer) under different stages of compression. White circles reveal a region that does not move much in the radial direction.



It has been shown that, when the ring length (thickness) equals the external to internal diameters difference, the traditional Kolsky expression for the material strength should be corrected to

$$s = 0.87 \frac{E_b A_b}{A_s} e_t.$$

Such a correction takes into account friction; no lubrication between the bars–material interfaces should be applied. We have here an important advantage of the use of ring specimens since it is literally impossible to perform a test with zero friction, specially in tests at high and low temperatures, as these extreme temperatures degrade the lubricant properties. We also mention that the strain rate in tests using rings tends to be more constant than when using disks. An example of how the rings perform is given in the next figure.

See M. Alves, D. Karagiozova, G.B. Micheli and M.A.G. Calle, Limiting the influence of friction on the split Hopkinson pressure bar tests by using a ring specimen, *International Journal of Impact Engineering*, 49, p.130–141, 2012.

7.5.3 Inertia and punching effects correction

In the same way energy is required to overcome friction, it is also a consequence of the EWM test that the sample will be accelerated in the thickness and radial direction. This energy causes an inertia effect, which is marginal in some cases. For instance, the measured stress level is affected by some 1% for copper.

The so called punching effect is also quite small. It arises due to the fact that a disk shape specimen tends to deform elastically the bars in the specimen–bar contact zone. This has been quantified, being found that it is more important when brittle materials are tested, where attention to small strains are necessary. For ductile materials, only at strains of less than say 1% this would be important.

See Displacement correction for punching at a dynamically loaded bar end, K. Safa and G. Gary, *International Journal of Impact Engineering*, 37, p.371–384, 2010.

with

$$[\bar{N}] = \{x\}[A]^{-1} = [1 - x/L_e \quad x/L_e]$$

being the shape function matrix.

The functional $\frac{1}{2} \int_0^{L_e} \sigma \varepsilon A dx$ becomes

$$\frac{EA}{2} \int_0^{L_e} \{u_1 \ u_2\} \frac{d[\bar{N}]^T}{dx} \frac{d[\bar{N}]}{dx} \{u_1 \ u_2\} dx$$

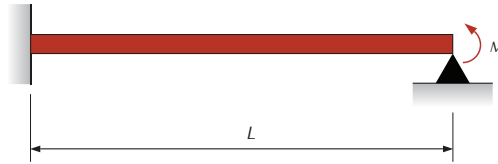
since $\varepsilon = \partial u / \partial x = d[\bar{N}] / dx \{u_1 \ u_2\}$. This axial degree of freedom should be incorporated in the right position of the stiffness matrix and load force, yielding the more complete beam finite element translated to the following algebraic system of equations

Note that torsion, which naturally arises in 3D frames, is not considered here.

$$\frac{E}{L_e} \begin{bmatrix} A & 0 & 0 & -A & 0 & 0 \\ 0 & \frac{12I}{L_e^2} & \frac{6I}{L_e} & 0 & -\frac{12I}{L_e^2} & \frac{6I}{L_e} \\ 0 & \frac{6I}{L_e} & 4I & 0 & -\frac{6I}{L_e} & 2I \\ -A & 0 & 0 & A & 0 & 0 \\ 0 & -\frac{12I}{L_e^2} & -\frac{6I}{L_e} & 0 & \frac{12I}{L_e^2} & -\frac{6I}{L_e} \\ 0 & \frac{6I}{L_e} & 2I & 0 & -\frac{6I}{L_e} & 4I \end{bmatrix} \begin{Bmatrix} u_1 \\ w_1 \\ \theta_1 \\ u_2 \\ w_2 \\ \theta_2 \end{Bmatrix} = \begin{Bmatrix} N_1 \\ F_1 \\ M_1 \\ N_2 \\ F_2 \\ M_2 \end{Bmatrix}.$$

Applying boundary conditions and loads

Let us now consider the hyperstatic problem of the beam in the next figure. The beam is represented by a single finite element. With this problem we will show how to impose boundary conditions and to apply concentrated loads to a finite element model.



A hyperstatic beam problem solved using a single FE.

Since the distributed loads, the transverse shear force and the normal force are all zero, the load vector reduces to

$$\begin{aligned} \{F_e\} &= \int_{L_e} p[\bar{N}] dx + \left[Q[\bar{N}] - M \frac{d[\bar{N}]}{dx} \right] \\ &= -M \frac{d[\bar{N}]}{dx} = [0 \quad 0 \quad 0 \quad -M]^T. \end{aligned}$$

equation and, for that, the finite strain variation is given by

$$\delta\varepsilon_x = \delta \left[\frac{du}{dx} + \frac{1}{2} \left(\frac{dw}{dx} \right)^2 + z\kappa \right] = \frac{d\delta u}{dx} + \frac{dw}{dx} \frac{d\delta w}{dx} - z \frac{d^2\delta w}{dx^2},$$

which, times the stress σ_x , results in

$$\delta W_{int} = \int \left[\left(\frac{d\delta u}{dx} + \frac{dw}{dx} \frac{d\delta w}{dx} \right) N - z \frac{d^2\delta w}{dx^2} M \right],$$

If we now collect the terms involving δu and δw and use the expressions for the external work, we obtain the so called weak forms

$$\int \frac{d\delta u}{dx} N = \int \delta u f dx + Q_1 \delta \Delta_1 + Q_4 \delta \Delta_4$$

and

$$\begin{aligned} & \int \left[\frac{d\delta w}{dx} \frac{dw}{dx} N - \frac{d^2\delta w}{dx^2} M \right] dx = \\ & = \int \delta w q dx + Q_2 \delta \Delta_2 + Q_3 \delta \Delta_3 + Q_5 \delta \Delta_5 + Q_6 \delta \Delta_6. \end{aligned}$$

An interesting remark here is that, from the above functional, *ie* from this weak form, we can obtain the equilibrium equation for the beam, as we have done using the so called vector approach. To this end, we need to eliminate the differentiation in the virtual displacements, which can be done by integration by parts of the above equations.

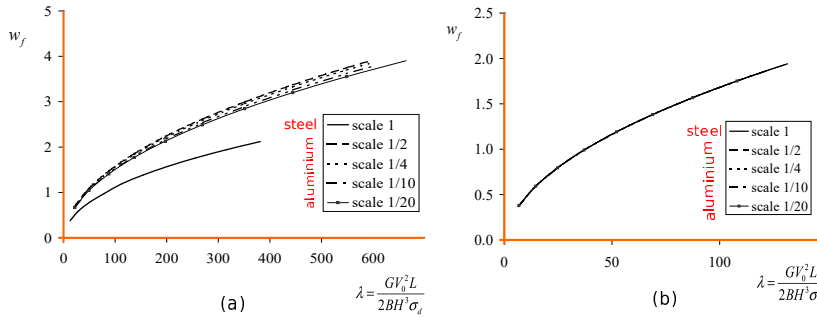
When the equilibrium equations obtained by the weak form and by the vector approach are the same, we refer to a consistent set of equilibrium equations, meaning that the assumed kinematic simplifications are consistent with the assumed simplification in the vector components of transverse shear force, normal force and bending moment.

Now that we have a consistent set of equilibrium equations, we can obtain the governing equation for the beam by joining the kinematic and stress fields via the material constitutive law, assumed here to be the linear one, *ie* $\sigma = E\varepsilon$. This will render the normal force and the bending moment as

$$N = \int E\varepsilon dA = A_1 \left[\frac{d\delta u}{dx} + \frac{1}{2} \left(\frac{d\delta w}{dx} \right)^2 \right]$$

and the smaller the scaling factor β , the larger the difference between the dimensionless mid-displacement of models and prototype. This is all expected since the usual scaling laws cannot cope with models and prototype made of different materials.

The figure also shows the same dimensionless mid-span beam displacement for the mild steel prototype and for the aluminium models but now subjected to the correction outlined before. It is rather evident and convincing that models and prototypes behave the same; indeed the error in this case is zero.



Mid-displacement evolution of an impacted clamped beam versus impact energy. (a) no correction, (b) corrected solution.



Consider now the temperature independent Johnson–Cook constitutive equation

$$\sigma_d = (A + B\epsilon^n) (1 + C \ln \dot{\epsilon}^*),$$

with ϵ being the equivalent plastic strain, $\dot{\epsilon}^* = \dot{\epsilon}/\dot{\epsilon}_0$ is the dimensionless plastic strain-rate for $\dot{\epsilon}_0 = 1/s$, a reference strain-rate, A , B , C and n material constants. We can write

$$\beta_\sigma = \frac{(A_m + B_m \epsilon_m^{n_m}) (1 + C_m \ln \dot{\epsilon}_m^*)}{(A_p + B_p \epsilon_p^{n_p}) (1 + C_p \ln \dot{\epsilon}_p^*)}$$

and, from $\dot{\epsilon}_p = (\beta/\beta_V)\dot{\epsilon}_m$, it follows that

$$\beta_\sigma = \frac{(A_m + B_m \epsilon_m^{n_m}) (1 + C_m \ln \dot{\epsilon}_m^*)}{(A_p + B_p \epsilon_p^{n_p}) \left(1 + C_p \ln \left(\frac{\beta \dot{\epsilon}_m^*}{\beta_V}\right)\right)} = \beta_{\sigma_0} \beta_{\sigma_d},$$

with

$$\beta_{\sigma_0} = \frac{A_m + B_m \epsilon_m^{n_m}}{A_p + B_p \epsilon_p^{n_p}},$$

$$\beta_{th}/\beta = 0.0588.$$

It is very important to realize that, in this specific case, the moving mass is the ship so, if the thickness is distorted, it is also the "impact mass" itself, and this should be taken into account.

10.8 Closure

The scaling laws were presented in this chapter to convey the important fact that it is possible to impact test large structures with the aid of small models. The results obtained from these models can be projected on the actual structure size if the right corrected scaling laws are observed.

The subject of scaling went so far that it is possible to work with a model whose not all dimensions are scaled by a single scaling factor β . This has important practical consequences since, as seen here, it is not possible to find a sheet thickness that scales as desired in many cases.

With the advent of 3D printing, it is also important to take note that new mathematical procedures dealing with the scaling laws allows one to test a structure model whose material is different from the prototype model. Although in its infancy, distorted scaling may well be an important aid to experimental mechanics, for inferring the behaviour of both very large and very small structures.

Having now a more comprehensive knowledge on impact engineering, we can move on to our last chapter, where various application of this engineering field will be explored.

10.9 Problems

1. For a clamped beam under a pulse velocity, obtain an expression for the scaled velocity such that the scaling is exact. Adopt the Norton law to describe the material strain rate sensitivity.
2. Obtain the variable force in the VSGd basis and show that it reduces to β^2 when there is no geometrical distortion or strain rate effects.
3. What are type I and type II structures? What would be the most appropriate of these structures to test scaling laws? Why?



(a)



(b)

a) Flexible road barrier made from steel and b) concrete barrier.

grade A, B or C. Grade A means low severity, while B and C are associated with a serious injury or even fatal to the car occupants. ASI is calculated by placing an (virtual) accelerometer in the car center of gravity. It is computed along the impact event and its maximum value and the maximum acceleration is used to evaluate it. If maximum ASI exceeds 1.0 or 1.4, then the impact event is considered very dangerous or lethal for the passengers. For THIV, the occupants head is considered to be a freely moving object that, as the vehicle changes its speed during contact with the road barrier it continues moving until it strikes a surface within the interior of the vehicle at a certain speed limit. The PHD describes the head deceleration after this impact.

Metallic guardrails composed by w-beam are installed with different cross section posts, like C shape, wood, etc. but here we explore only the so called sigma post placed every 2 m along the guardrail. The inclusion of the soil and their property adds flexibility to the metallic guardrail and makes the behaviour of the system closer to the real installations on highways. The deformable vehicle model with 25037 finite elements is based on a commercial vehicle obtained in the NCAC database. It is a light vehicle of 894 kg with no passengers, as shown in the next figure.